Mechanical and tribological properties of Fe/Cr–$FeAl_2O_4$–Al_2O_3 nano/micro hybrid composites prepared by spark plasma sintering

J. Gurt Santanach, C. Estournès, A. Weibel, A. Peigney, G. Chevallier and Ch. Laurent*

CIRIMAT, UMR CNRS-UPS-INP 5085, Bât. 2R1, Université Paul-Sabatier, 31062 Toulouse cedex 9, France

Fe/Cr–Al_2O_3 nanocomposite powders are prepared by H_2 selective reduction of oxide solid solutions. These powders, an alumina powder and a starting oxide powder, are sintered by spark plasma sintering. The microstructure of the resulting materials is studied. The composites show a lower microhardness and higher fracture strength than unreinforced alumina. The friction coefficient against an alumina ball is lower, revealing the role of the intergranular metal particles, whereas $FeAl_2O_4$ grains formed during SPS are beneficial for higher cycle numbers.

Keywords: Spark plasma sintering; Particulate reinforced composites; Alumina; Nanocomposite; Friction

Metal–oxide (ceramic–matrix) micro- and nanocomposites have been studied for decades. The main aim of the studies was to prepare stronger and tougher materials, owing notably to the ability of the metal particles to deform plastically and bridge cracks, deflect cracks and hamper microcrack propagation by absorbing some of the associated energy by elastic deformation. Alumina–matrix nanocomposites and nano/micro hybrid composites showing high strength and toughness were reported [1–7] in the 1990s. Comparing earlier [8,9] and more recent [10,11] review articles reveals that there has been little progress since that time but the latter works point out that such materials could be interesting for tribological applications. Dutta et al. [12] reported that abrasion and plastic deformation are the primary operative wear mechanisms in the Ag–Al_2O_3 microcomposites. Oh et al. [13] reported that the friction coefficient of Ni/Co–Al_2O_3 nanocomposites is slightly higher than that of Al_2O_3. de Portu et al. [14] reported that the friction coefficient against a hard WC pin of Mo–Al_2O_3 and Nb–Al_2O_3 microcomposites decreases when increasing the applied load. The wear resistance of Mo–Al_2O_3 composites is low because of the low adherence of particles to the matrix. The presence of molybdenum oxides formed during the test could help to lower the friction coefficient. Nb–Al_2O_3 microcomposites are more wear-resistant because the Nb particles are more difficult to extract. Fe/Cr–Al_2O_3 nanocomposites containing both intragranular and intergranular metal microparticles [1–3,15] and consolidated by spark plasma sintering (SPS) were studied in fretting conditions against Ti–6Al–4V [16]. It was notably shown that the intergranular particles improve the wear resistance because they limit the pull-out of the matrix grains. In this paper, we study the influence on the friction coefficient of the metal content, and hence of the microstructure, of $Fe_{0.8}Cr_{0.2}$–Al_2O_3 composites consolidated by SPS.

Powders of α–Al_2O_3 (corundum-type structure) and α-$Al_{2-2x}(Fe_{0.8}Cr_{0.2})_{2x}O_3$ ($x = 0.07$; 0.10 and 0.20) were prepared by the mixed-oxalate precipitation/calcination route [15]. The calcination (air, 1200 °C, 2 h) produced powders in which micrometric grains form agglomerates 15–20 μm in size, presenting a vermicular microstructure. It was verified by X-ray diffraction (XRD, Cu K_α radiation, Bruker D4 Endeavor, not shown) that only the peaks typical of the corundum-type oxide are present. However, for the powder with $x = 0.20$, XRD revealed the peaks of a hematite-rich solid solution (α_2) in addition to the alumina-rich solid solution (α_1), which indicates that the supersaturation of hematite dissolved into the alumina-chromia solid solution was reached for this sample (i.e. that the limit of substituting Fe^{3+} ions for Al^{3+} ions in the corundum lattice was reached) [17]. These powders were selectively reduced in pure H_2 (1300 °C, 1 h) in order to produce Fe/Cr–Al_2O_3 nanocomposite powders where the metal particles are located both at the surface of and within the α-Al_2O_3 grains [15]. The nanocomposite powders prepared from the oxides with $x = 0.07$, 0.10 and 0.20 are denoted FC7, FC10 and FC20, respectively. XRD (not shown) revealed only

* Corresponding author. E-mail: laurent@chimie.ups-tlse.fr

doi:10.1016/j.scriptamat.2010.12.042

peaks typical of the corundum-type oxide for all powders and also the (1 1 0) peak of α-Fe/Cr, with an increasing proportion for FC7, FC10 and FC20. A total reduction would yield metallic particles with the $Fe_{0.8}Cr_{0.2}$ composition, but previous studies showed that, because the Fe^{3+} and Cr^{3+} cations have different reducibilities, the surface particles tend to be richer in iron than the target composition whereas the intragranular ones tend to be richer in chromium [18]. In addition, the matrix is not strictly α-Al_2O_3 but rather a α-Al_2O_3-Cr_2O_3 solid solution. The powders were observed by transmission electron microscopy (TEM; JEOL JEM 1011). Typical TEM images (Fig. 1) reveal metal nanoparticles about 20 nm in diameter (arrowed on Fig. 1) located in the pores of the oxide matrix and smaller nanoparticles (<10 nm), which are extremely numerous. Although such images do not allow one to determine if the latter nanoparticles are at the surface or within the oxide grains, an earlier electron microdiffraction study [19] revealed that virtually all are within, i.e. in an intragranular position. These nanoparticles are smaller for FC7 (Fig. 1a) than for FC20 (Fig. 1b). The composite powders were studied by thermogravimetric analysis (TGA, Setaram TAG 24) in flowing air up to 1400 °C (heating rate 3 °C min^{-1}) in order to oxidize the metal nanoparticles (Fig. 2). The maximum weight gain w_{max} is 1.45, 2.97 and 6.83% for FC7, FC10 and FC20, respectively. Comparing these values to those that would have been obtained if the Fe^{3+} and Cr^{3+} ions had been reduced to metallic Fe and Cr, respectively, gives reduction yields of 54, 77 and 88%. Thus, the real metal content is 3.8, 7.7 and 17.6 wt.% for FC7, FC10 and FC20, respectively. The TGA curves and the corresponding derivative curves (not shown) show that the oxidation occurs in at least three steps. It has been shown previously [20] that the steps at ca. 600 and 900 °C correspond to the oxidation of the metal nanoparticles located onto the surface and into the open porosity of the oxide grains, respectively, whereas the latter step (ca. 1200 °C) corresponds to the oxidation of the intragranular nanoparticles. Comparing the weight gain at 600 °C to w_{max} indicates that the proportion of the metallic phase at the surface of the Al_2O_3 grains is about 20, 48 and 65% for FC7, FC10 and FC20, respectively. After sintering, the corresponding particles will be in intergranular position and it is estimated that the metallic phase proportion (*P*, Table 1) will be the same than in the powders.

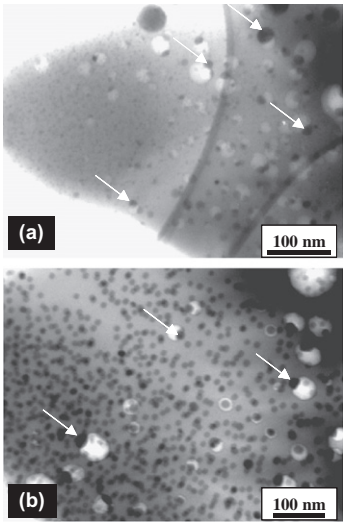

Figure 1. TEM images of the FC7 (a) and FC20 (b) nanocomposite powders.

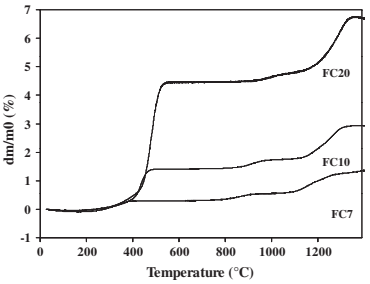

Figure 2. TGA curves (air) for the FC7, FC10 and FC20 nanocomposite powders.

The four powders were consolidated by SPS (Dr. Sinter 2080, SPS Syntex Inc., Japan). They were loaded into a 20 mm inner diameter graphite die. A sheet of graphitic paper was placed between the punch and the powder as well as between the die and the powder for easy removal. This ensemble is known as the stack. The powders were sintered in vacuum (residual cell pressure about 5 Pa). A pulse configuration of 12 pulses (one pulse duration 3.3 ms) followed by two periods (6.6 ms) of zero current was used. Heating rates of 200 and 250 °C min^{-1} were used from room temperature to 600 °C and from 600 to 1350 °C, respectively. A dwell of 3 min was applied at 1350 °C. An optical pyrometer, focused on a little hole at the surface of the die, was used to measure the temperature. A uniaxial pressure of 150 MPa was progressively applied from 950 °C up to the dwell temperature. Cooling rate was 100 °C min^{-1}. The uniaxial pressure was gradually released during cooling. The sintered specimens, designated FC7S, FC10S and FC20S in the following, were in form of pellets 20 mm in diameter and about 2 mm thick. They were polished down to 1 μm using diamond suspensions. The density determined by the Archimedes method (Table 1) corresponds to a densification of about 98% for all specimens.

The XRD patterns (not shown) of the surfaces of FC7S, FC10S and FC20S reveal the peaks of three species. Besides the corundum-type phase and the metal, there is a spinel-type phase ($FeAl_2O_4$) with relatively intense peaks, which increase with increasing metal content. The formation of $FeAl_2O_4$ during the SPS of α-$Al_{2-2x}Fe_{2x}O_3$ solid solutions and Fe–α-$Al_{2-2y}Fe_{2y}O_3$ nanocomposites was previously shown [21] to involve a Fe (III) → Fe (II) reaction due to the reducing conditions during the SPS treatment and also a retrodismutation of iron, Fe(0) + Fe(III) → -Fe(II). The polished surfaces were observed by field-emission-gun scanning electron microscopy (FESEM; JEOL JSM 6700F) (Fig. 3a and b). In such images (back-scattered electron images in chemical composition mode), the intergranular metal particles appear as white dots and the spinel phase as light-gray grains on a dark-gray background of the corundum-phase matrix. The metal particles are homogeneously distributed in the matrix. Their average diameter, evaluated by measuring the diameter of about 100 particles on such images, is in the range 0.4–0.6 μm, increasing only slightly with increasing metal content (*d*, Table 1), indicating that exaggerated coalescence

Table 1. Density (ρ), matrix grain size (D), intergranular metal particles size (d), proportion of intergranular metallic phase (P) as deduced from TGA (see text for details), fraction of surface area occupied by metal particles (S_m), fraction of surface area occupied by spinel grains (S_s), fracture strength (σ_f), toughness (K_{Ic}) and Vickers microhardness (HV) for the alumina and nanocomposite materials prepared by SPS.

Specimen	ρ (g.cm^{-3})	D (μm)	d (μm)	P (%)	S_m (%)	S_s (%)	σ_f (MPa)	K_{Ic} (MPa.m$^{1/2}$)	HV (GPa)
Al_2O_3	3.89	2.2 ± 0.2	–	–	–	–	446 ± 60	3.8 ± 0.5	19.0.0 ± 0.5
FC7S	4.01	2.1 ± 0.2	0.4 ± 0.2	20	2.6	1.1	524 ± 60	3.8 ± 0.5	17.9 ± 0.5
FC10S	4.06	2.1 ± 0.2	0.5 ± 0.1	48	2.8	1.7	532 ± 60	4.0 ± 0.5	17.6 ± 0.5
FC20S	4.32	2.1 ± 0.2	0.6 ± 0.1	65	5.1	3.9	637 ± 60	4.4 ± 0.5	17.3 ± 0.5

was prevented. The spinel grains are similarly sized. The proportion of surface area occupied by the metal particles, also determined by analysis of FESEM images, is about 2.6%, 2.8% and 5.1% for FC7S, FC10S and FC20S, respectively (S_m, Table 1). The proportion of surface area occupied by the spinel grains is lower but follows a similar evolution (S_s, Table 1).

The indentation tests (10 N for 10 s in air at room temperature) were performed on the polished surface of the specimens by loading with a Vickers indenter (Shimadzu HMV 2000). The calculated microhardness values (Table 1) are the average of 10 measurements. The Vickers microhardness (HV) decreases regularly upon the increase in metal content, from 19.0 GPa for Al_2O_3 to 17.30 GPa for FC20S. This could show that the surface behaviour reflects the presence of the metal particles. Indeed, the solid solution hardening observed by Bradt [22] for α-Al_2O_3–Cr_2O_3 is not observed. The transverse fracture strength (σ_f) was determined by the three-point bending test on ($1.6 \times 1.6 \times 18$ mm^3) specimens machined with a diamond blade. The cross-head speed was fixed at 0.1 mm min^{-1}. σ_f (Table 1) increases from Al_2O_3 to FC20S. The values are lower than those reported previously for hot-pressed specimens [1,3,9], which could reflect

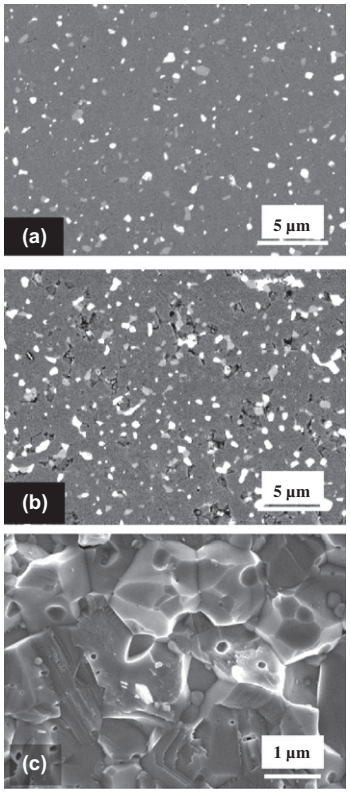

Figure 3. FESEM image of the polished surface of FC10S (a) and FC20S (b) and of the fracture surface of FC10S (c).

the presence of the spinel phase. It has been reported [23] that nano- and microprecipitates of $FeAl_2O_4$ increase the fracture strength of Al_2O_3 and the present values tend to be slightly higher, notably for FC20S. The fracture toughness (K_{Ic}) was measured by the single edge-notched bend (SENB) method on similar specimens notched using a 100 μm SiC wire. A calibration factor [24] was used to calculate the SENB toughness from the experimental results. K_{Ic} (Table 1) is similar for all specimens. This could reflect the presence of more spinel than metal in the core of the materials, making them more or less similar to each other. Indeed, the notch is deep enough so that only the core is tested. The present values are in good agreement with those reported [23] for $FeAl_2O_4$–Al_2O_3 nanocomposites. The size of the Al_2O_3 grains was evaluated on FESEM images of the fracture surfaces (Fig. 3c) and is similar (about 2.1 μm) for all samples (Table 1). The fracture mode is mixed, transgranular and intergranular, as was previously observed for metal–Al_2O_3 nanocomposites prepared by hot-pressing, for which it was shown that the presence of intragranular metal nanoparticles resulted in a transgranular fracture, even for micrometric alumina [1–7].

The dry friction experiments were performed using a ball-on-reciprocating flat geometry. An alumina ball (TCP-C-AA-0063, CSM, Switzerland) 6 mm in diameter was used against flat sample surfaces. The normal load was fixed at 5 and 10 N and the sliding speed was fixed at 5 cm s^{-1}. The reciprocating stroke was 20 mm and the test was performed for 1592 cycles. The frictional force transferred to a load cell was recorded throughout the tests. For a load of 5 N, the friction coefficient (not shown) for the three nanocomposites (0.28–0.35) is lower than that obtained for Al_2O_3 (>0.40). The differences between the nanocomposites are not significant, possibly because of the moderate load. For a load of 10 N (Fig. 4), the friction coefficient for the nanocomposites is again lower than for Al_2O_3. Interestingly, below about 350 cycles, it is much lower when the metal content is higher. Moreover, the contact stabilization is slower when the metal content increases. Indeed, the friction coefficient is constant (0.33) above 200 and 500 cycles for FC7S and FC10S, respectively, whereas it is stabilized (0.36) over 1000 cycles for FC20S. The wear is negligible at the end of the test whatever the composition of the specimens. However, the wear of the alumina ball, which is very low for both FC7S and FC10S, appears slightly higher for FC20S. These results could be correlated with the metal content, the amount of intergranular metal particles (P, Table 1) and the proportion of surface area occupied by these particles (S_m, Table 1), which both increase with increasing metal content, and to the corresponding decrease in microhardness. The much lower friction coefficient at the beginning of the test could reflect the lubricating role of the intergranular

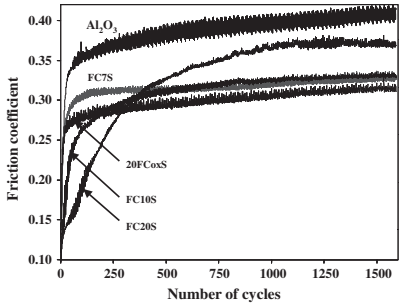

Figure 4. Friction coefficient vs. number of cycles for an applied load of 10 N.

metal particles. This effect is more marked for FC20S because the proportion of surface area occupied by such particles is almost double that for FC7S and FC10S.

However, this specimen being slightly less hard than the others, an increase in the number of cycles could cause some pulling-out of the metal particles, which may also oxidize, resulting in a higher deterioration of the alumina ball. This could result in too much contact between the composite and the alumina ball, and thus in a slower stabilization and a higher friction coefficient. However, the friction behaviour of alumina [25–30] and metal–alumina composites [12–14,16] depends strongly on the test conditions, and a more detailed analysis is required to supplement this preliminary study. A recent study [23] suggested that metal particles may be detrimental for wear-resistant applications and that $FeAl_2O_4$–Al_2O_3 composites may be more desirable. Thus, an oxide powder prepared with $x = 0.20$, thus made up of a mixture of α_1 and α_2, was densified by SPS (sample denoted 20FCoxS). XRD patterns (not shown) of the surface reveal the peaks of the corundum-type phase and of $FeAl_2O_4$. From FESEM images, it was found that the matrix grain size is 0.8 ± 0.2 μm and that spinel grains, representing ca. 18% of the surface, are elongated (ca. 1.7×0.7 μm^2). HV is equal to 17.9 ± 1.0 GPa (similar to FC7S). At the beginning of the friction test (Fig. 4), 20FCoxS behaves like FC7S, but the friction coefficient is stabilized at a slightly lower value. Thus, the benefit of metal particles could be found only for small displacements, whereas that of the $FeAl_2O_4$ grains could be found for a higher number of cycles.

In conclusion, Fe/Cr–Al_2O_3 composite powders with different metal contents (3.8, 7.7 and 17.6 wt.%) were prepared by selective reduction in H_2 of the corresponding α-$Al_{2-2x}(Fe_{0.8}Cr_{0.2})_{2x}O_3$ solid solutions. These powders, an alumina powder and a starting oxide powder, were sintered by SPS. The sintered composites contain intragranular metal nanoparticles and intergranular submicrometric metal particles as well as in situ formed $FeAl_2O_4$ grains, dispersed in a corundum-phase matrix. The proportion of the intergranular metal particles and the corresponding proportion of occupied surface area increase with increasing metal content. The composites show a lower microhardness, higher fracture strength and similar toughness than the unreinforced alumina. The friction coefficient against an alumina ball is lower for the composites, most notably below about 350 cycles, for increasing metal content. For the composite with 3.8 wt.% of metal, the friction system become almost stationary after about 200 cycles, with a friction coefficient significantly lower than alumina. Wear appears to be negligible. The oxide powder ($x = 0.20$) sintered without prior reduction shows a friction behaviour almost similar to that of the composite containing 3.8 wt.% of metal and a still lower friction coefficient. These results could reveal the lubricating role of the submicrometric intergranular metal particles for low displacements, whereas the beneficial role of $FeAl_2O_4$ grains is dominant for higher numbers of cycles. The microstructure is complex and more studies are necessary to fully understand the tribological behaviour.

The authors thank L. Datas for assistance in the TEM observations, performed at TEMSCAN, the "Service Commun de Microscopie Electronique à Transmission", Université Paul-Sabatier. The SPS was performed at the Plateforme Nationale CNRS de Frittage-Flash (PNF^2, Toulouse). The authors thank Y. Paranthoen (Société des Céramiques Techniques, Bazet, France) for a J.G.S. doctoral thesis grant. This work is performed under the programme ANR-06-NANO-049.

[1] X. Devaux, Ch. Laurent, M. Brieu, A. Rousset, C. R. Acad. Sci. Paris, Série II 312 (1991) 1425.
[2] Ch. Laurent, X. Devaux, A. Rousset, J. High Temp. Chem. Process. 3 (1994) 489.
[3] A. Rousset, J. Solid State Chem. 111 (1994) 164.
[4] K. Niihara, A. Nakahira, T. Sekino, Mater. Res. Soc. Symp. Proc. 286 (1993) 405.
[5] M. Nawa, T. Sekino, K. Niihara, J. Mater. Sci. 29 (1994) 3185.
[6] T. Sekino, K. Niihara, Nanostruct. Mater. 6 (1995) 663.
[7] T. Sekino, K. Niihara, J. Mater. Sci. 32 (1997) 3943.
[8] Ch. Laurent, A. Rousset, Key Eng. Mater. 108–110 (1995) 405.
[9] C. Laurent, A. Peigney, O. Quénard, A. Rousset, Sil. Ind. 63 (1998) 77.
[10] J.S. Moya, S. Lopez-Esteban, C. Pecharroman, Prog. Mater. Sci. 52 (2007) 1017.
[11] J.A. Yeomans, J. Eur. Ceram. Soc. 28 (2008) 1543.
[12] A.K. Dutta, A.B. Chattopadhyaya, K.K. Ray, Wear 261 (2006) 885.
[13] S.T. Oh, S.J. Yoon, Y.H. Choa, Y.K. Jeong, K. Niihara, Key Eng. Mater. 317–318 (2006) 369.
[14] G. de Portu, S. Guicciardi, C. Melandri, F. Monteverde, Wear 262 (2007) 1346.
[15] X. Devaux, Ch. Laurent, A. Rousset, Nanostruct. Mater. 2 (1993) 339.
[16] P. Stempflé, F. Pollet, L. Carpentier, Tribol. Int. 41 (2008) 1009.
[17] A. Muan, S. Somyia, J. Am. Ceram. Soc. 42 (1959) 603.
[18] Ch. Laurent, J.-J. Demai, A. Rousset, K.R. Kannan, C.N.R. Rao, J. Mater. Res. 9 (1994) 229–235.
[19] X. Devaux, Ch. Laurent, M. Brieu, A. Rousset, J. Alloys Compd. 188 (1992) 179.
[20] Ch. Laurent, Ch. Blaszczyk, M. Brieu, A. Rousset, Nanostruct. Mater. 6 (1995) 317.
[21] J. Gurt Santanach, C. Estournès, A. Weibel, A. Peigney, G. Chevallier, Ch. Laurent, Scripta Mater. 60 (2009) 195.
[22] R.C. Bradt, J. Am. Ceram. Soc. 50 (1967) 54.
[23] A. Mukhopadhyay, R.I. Todd, J. Eur. Ceram. Soc. 30 (2010) 1359.
[24] W.F. Brown, J.E. Srawley, ASTM Spec. Tech. Pub. 10 (1966) 13.
[25] H. Hong, W.O. Winer, J. Tribol. 111 (1989) 504.
[26] Y.S. Zhou, M. Ohashi, K. Ikeuchi, Wear 210 (1997) 112.
[27] J.D.O. Barceinas-Sanchez, W.M. Rainforth, Acta Mater. 46 (1998) 6475.
[28] H. Dong, T. Bell, Wear 225–229 (1999) 874.
[29] A. Ravikiran, S. Jahanmir, Wear 251 (2001) 980.
[30] R.S. Mishra, A.K. Mukherjee, Mater. Sci. Eng. A 301 (2001) 97.